Electrostatics in periodic boundary conditions and real-space corrections

Ismaila Dabo,[1,*] Boris Kozinsky,[2] Nicholas E. Singh-Miller,[1] and Nicola Marzari[1]
[1]*Department of Materials Science and Engineering, Massachusetts Institute of Technology, Cambridge, Massachusetts 02139, USA*
[2]*Department of Physics, Massachusetts Institute of Technology, Cambridge, Massachusetts 02139, USA*
(Received 27 September 2007; published 27 March 2008)

We address periodic-image errors arising from the use of periodic boundary conditions to describe systems that do not exhibit full three-dimensional periodicity. The difference between the periodic potential, as straightforwardly obtained from a Fourier transform, and the potential satisfying any other boundary conditions can be characterized analytically. In light of this observation, we present an efficient real-space method to correct periodic-image errors, based on a multigrid solver for the potential difference, and demonstrate that excellent convergence of the energy with respect to cell size can be achieved in practical calculations. Additionally, we derive rapidly convergent expansions for determining the Madelung constants of point-charge assemblies in one, two, and three dimensions.

DOI: 10.1103/PhysRevB.77.115139 PACS number(s): 71.15.−m, 31.15.−p, 31.70.−f

I. INTRODUCTION

First-principles calculations frequently employ periodic boundary conditions and plane-wave basis sets to determine the electronic structure and properties of materials. Besides being the most appropriate choice for the study of crystalline systems, this computational approach allows the use of highly optimized fast Fourier transform (FFT) algorithms,[1–3] which minimize the cost associated with the solution of the electrostatic equations, the calculation of electronic kinetic energies, and the determination of interatomic forces. Despite these advantages, periodic-boundary-condition calculations require large unit cells when studying nonperiodic or partially periodic systems (e.g., isolated molecules, polymer chains, or crystal slabs) in order to minimize spurious electrostatic interactions between periodic images. Charged systems are particularly problematic since their electrostatic energy would be divergent; conventional algorithms automatically impose a charge-neutrality condition, implicitly introducing an artificial jellium background.[4] As shown by Makov and Payne,[5] these artifacts induce significant energy errors scaling in three dimensions as $1/L^3$ for isolated neutral systems and $1/L$ for charged ones, where L denotes the size of the unit cell.

Several schemes have been devised to reduce periodic-image errors. In an approach first discussed by Barnett and Landman,[6] Marx *et al.*,[7] and Marx and Hutter,[8] periodic-image interactions for cluster systems are eliminated by restricting the plane-wave expansions of the wave functions and of the charge density to a spherical domain in reciprocal space. A generalization of this reciprocal-space scheme was later introduced by Martyna and Tuckerman.[9] The electrostatic-cutoff approach by Jarvis *et al.*[10] suppresses periodic-image effects by damping the electrostatic potential beyond a certain interaction range. Rozzi *et al.*[11] introduced an extension of this electrostatic-truncation approach to partially periodic systems. A similar generalization was proposed by Ismail-Beigi.[12] The corrective method introduced by Blöchl consists of using atom-centered Gaussian charges and Ewald summation techniques to cancel periodic-image interactions.[13] In the related, local-moment-countercharge (LMCC) method developed by Schultz,[14] a superposition of Gaussians is employed as a local-moment model for analytically calculating the Coulomb potential up to a certain multipole order; the remaining electrostatic contribution is computed using conventional plane-wave techniques. Considering atomic adsorption on neutral slabs, Neugebauer and Scheffler[15] proposed eliminating the adsorbate-induced polarization through the introduction of a counteracting planar dipole between slab images using the linear- and planar-average approximations proposed by Baldereschi *et al.*[16] Refinements of this method were subsequently developed.[17–19] Extending this approach to charged surfaces, Lozovoi and Alavi[20] inserted a charged Gaussian layer in vacuum to compensate for the excess charge and to allow electric-field discontinuities across the layer.

In this work, we propose an alternative approach for correcting periodic-image errors and show that excellent energy convergence with respect to cell size can be obtained at tractable computational costs. The approach proceeds by considering the exact electrostatic potential in open-boundary conditions (or any other boundary condition) as the sum of the periodic solution to the Poisson equation—computed using inexpensive FFT techniques—and a real-space correction that can be obtained accurately and inexpensively on coarse-grained meshes with multigrid techniques. In the following sections, we first discuss and characterize the difference between the open-boundary electrostatic potential and its periodic counterpart, providing a comparative basis for analyzing the relative accuracy of various corrective schemes. Second, we present our correction method and assess its performance. Last, we extend the method to the study of systems exhibiting one- or two-dimensional periodicity beyond the conventional linear- and planar-average approximations.

II. COMPARISON OF THE OPEN-BOUNDARY AND PERIODIC POTENTIALS

A. Definition of the corrective potential

The electrostatic potential v generated by an isolated charge distribution ρ satisfies the Poisson equation,

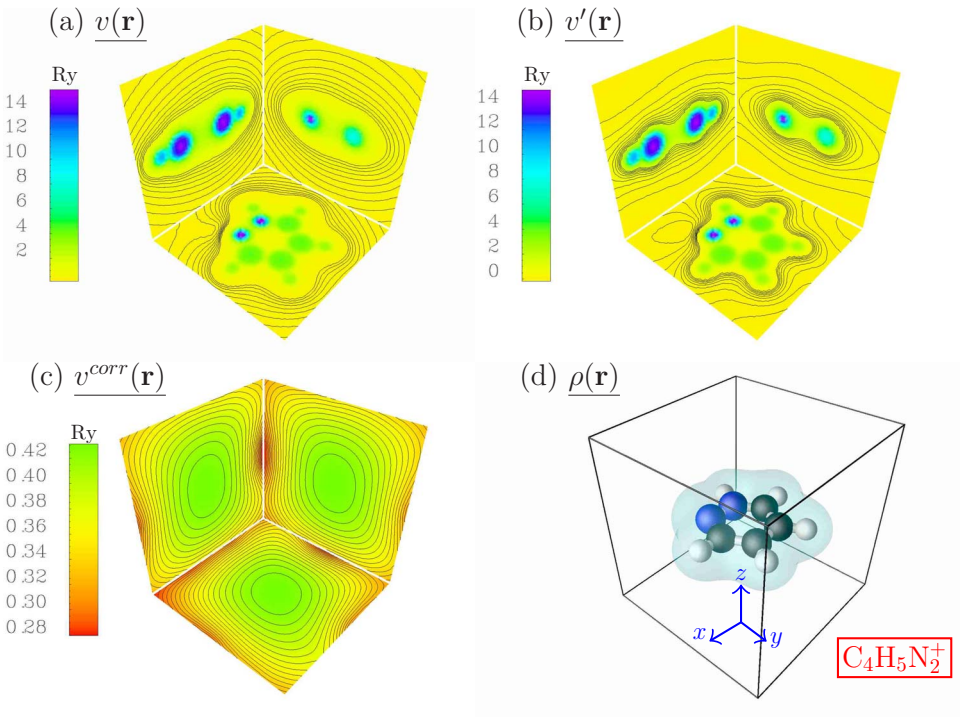

FIG. 1. (Color online) (a) Open-boundary electrostatic potential v, (b) periodic electrostatic potential v', and (c) electrostatic-potential correction $v^{\mathrm{corr}}=v-v'$ for a pyridazine cation in a cubic cell of length $L=15$ bohr. The potentials are plotted in three orthogonal planes (Oxy), (Oxz), and (Oyz) passing through the center of the cell.

$$\nabla^2 v(\mathbf{r}) = -4\pi\rho(\mathbf{r}) \tag{1}$$

(a.u. are used throughout). In the absence of an external electric field, we can solve Eq. (1) subject, e.g., to open-boundary conditions (that is, $v(\mathbf{r})\to 0$ as $|\mathbf{r}|\to+\infty$), which yield the integral expression for the solution,

$$v(\mathbf{r}) = \int \frac{\rho(\mathbf{r}')}{|\mathbf{r}-\mathbf{r}'|} d\mathbf{r}'. \tag{2}$$

(Although this study focuses on open-boundary conditions, other boundary conditions or contributions from an external electric field[18,21,22] could also be considered.)

A differential equation similar to Eq. (1) can be written for the potential v', satisfying periodic-boundary conditions, and generated by a periodic translation of the same charge distribution ρ. Keeping in mind that periodic boundary conditions can only accommodate a net zero charge (as seen from Gauss' law), we have

$$\nabla^2 v'(\mathbf{r}) = -4\pi(\rho(\mathbf{r}) - \langle\rho\rangle). \tag{3}$$

The periodic potential v' can be evaluated in reciprocal space as

$$v'(\mathbf{r}) = \sum_{\mathbf{g}\neq\mathbf{0}} \frac{4\pi}{\mathbf{g}^2}\rho(\mathbf{g})e^{i\mathbf{g}\cdot\mathbf{r}}, \tag{4}$$

where we set the arbitrary component $v'(\mathbf{g}=\mathbf{0})=\langle v'\rangle$ to zero.

The open-boundary potential v and its periodic counterpart v' are different, and here we define the corrective potential v^{corr} to the periodic solution as $v-v'$. The potential v^{corr} satisfies the much simpler, smoother differential equation,

$$\nabla^2 v^{\mathrm{corr}}(\mathbf{r}) = -4\pi\langle\rho\rangle, \tag{5}$$

although with Dirichlet conditions at the cell boundaries, as given by the difference between the open-boundary and periodic potentials. (Note that the solution of this simple elliptic boundary value problem is uniquely defined.) Equation (5) indicates that the curvature of the corrective potential is a constant. Additionally, apart from the value of the average $\langle\rho\rangle$, Eq. (5) is independent of the structural details of the charge density ρ. These details are entirely embedded in the Dirichlet boundary conditions, which reflect the electrostatic contributions from the compensating jellium and from the surrounding images.

In order to illustrate the implications of Eq. (5), we consider a pyridazine cation in a periodically repeated cubic cell. The open-boundary potential v, the periodic potential v', and the corrective potential v^{corr} are shown in Fig. 1. First, we observe that the potential v' is shifted in energy with respect to v due to the fact that the average $\langle v'\rangle$ is null by construction. In addition to this energy shift, the potential v' is significantly distorted. This distortion results from satisfying the periodicity conditions. Most importantly, we observe that the corrective potential v^{corr} varies smoothly over space. The smooth spatial dependence of v^{corr} contrasts markedly with the strong variations in v and v'. Performing a polynomial regression, we can verify that the potential v^{corr} is quadratic to a good approximation in the proximity of the cell center with departures from parabolicity restricted to the vicinity of the periodic boundaries.

To further examine the characteristics of v^{corr}, we consider the adsorption of carbon monoxide molecules on neutral and charged platinum slabs. Following Neugebauer and Scheffler,[15] the electrostatic correction is calculated along the z direction within the planar-average approximation (that is,

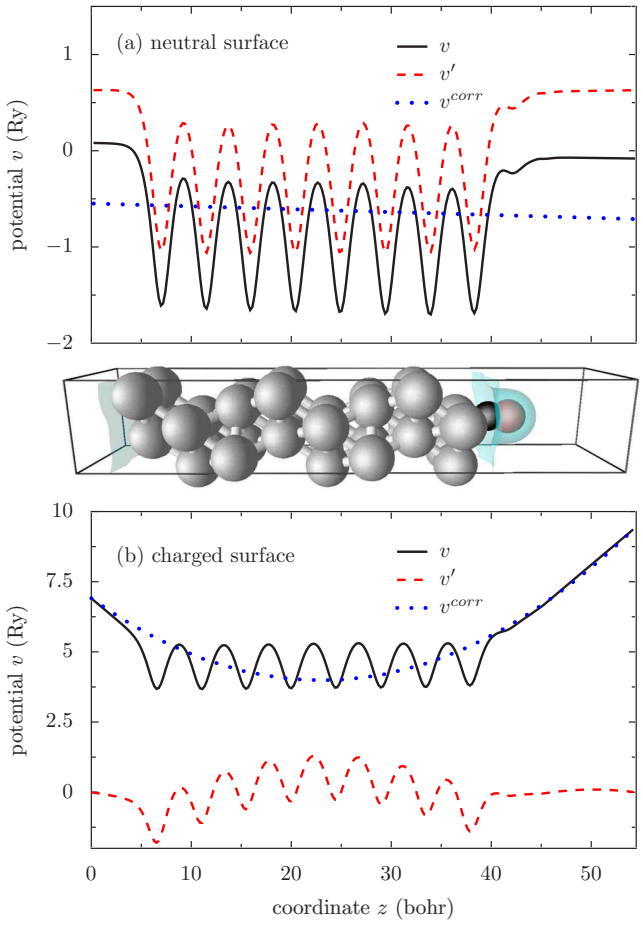

FIG. 2. (Color online) Open-boundary electrostatic potential v, periodic potential v', and electrostatic-potential correction v^{corr} averaged in the xy plane parallel to the surface for (a) carbon monoxide adsorbed on a neutral platinum slab and (b) carbon monoxide adsorbed on a charged platinum slab.

from the xy average of the charge distribution). The validity of this approximation is discussed in the last section. For CO molecules adsorbed on a neutral slab [Fig. 2(a)], the periodic potential is shifted up in energy and tilted with respect to the open-boundary potential. The potential correction is seen to be linear, which is in agreement with the analysis of Neugebauer and Scheffler.[15] For CO molecules adsorbed on a slab of surface charge $\tilde{\sigma}$ [Fig. 2(b)], the real-space potential diverges as $4\pi\tilde{\sigma}|z|$ (in the absence of an external electric field). In this case, the periodic potential v' undergoes a significant energy downshift, which decreases the energy of the positively charged slab. Moreover, we observe that v' is significantly curved in the slab region. Consistent with these observations and with Eq. (5), the corrective potential v^{corr} is found to be parabolic everywhere in the unit cell.

B. Quasiparabolic behavior of the corrective potential

In order to complete the analysis of the corrective potential, we consider a point charge $q=+e$ in a periodically repeated cubic cell of length L, as illustrated in Fig. 3. The corrective potential generated by the uniform jellium and the

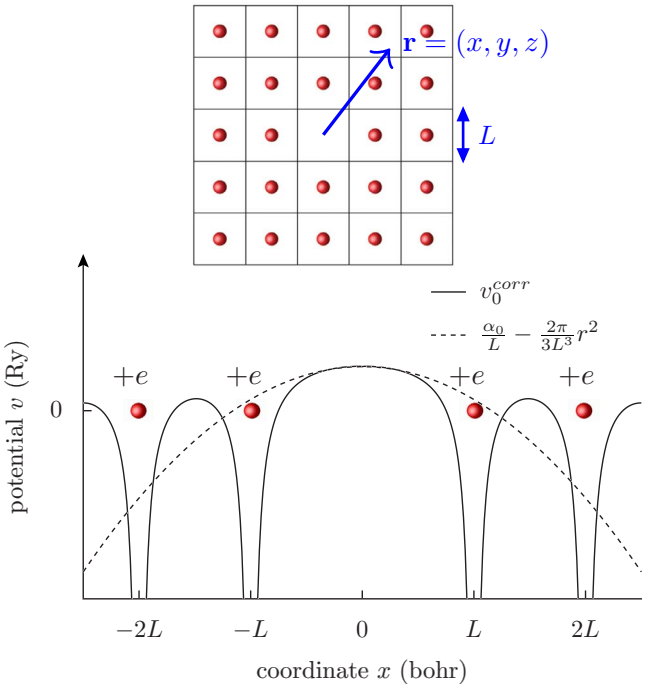

FIG. 3. (Color online) Corrective potential v_0^{corr} for a cubic lattice of point charges and its parabolic approximation in the vicinity of the origin.

surrounding point charges is denoted by v_0^{corr}. Note that v_0^{corr} cannot be calculated directly as the difference between the potential of a lattice of point charges v_0' and the point-charge potential $1/r$ since the representation of a point charge in reciprocal space requires an infinite number of plane-wave components. Instead, to obtain v_0^{corr}, we can exploit the cubic symmetry of the system by writing the corrective potential as

$$v_0^{\mathrm{corr}}(\mathbf{r}) = v_0^{\mathrm{corr}}(0) + \nabla^2 v_0^{\mathrm{corr}}(0)\frac{r^2}{6} + O(|\mathbf{r}|^4). \tag{6}$$

This parabolic expansion, valid up to third order, confirms that the point-charge correction v_0^{corr} is almost quadratic in the vicinity of $r=0$. For noncubic lattices, due to inversion symmetry, the point-charge corrective potential can be expressed as

$$v_0^{\mathrm{corr}}(\mathbf{r}) = v_0^{\mathrm{corr}}(0) + \sum_{\alpha} \frac{\partial^2 v_0^{\mathrm{corr}}}{\partial x_\alpha^2}(0)\frac{x_\alpha^2}{2} + O(|\mathbf{r}|^4) \tag{7}$$

(where x_α are the coordinates of $\mathbf{r}$ along the principal axes). Thus, the corrective potential in a noncubic lattice is also quadratic to the third order.

Turning now to an arbitrary distribution ρ, we can express the electrostatic correction v^{corr} by superposition,

$$v^{\mathrm{corr}}(\mathbf{r}) = \int v_0^{\mathrm{corr}}(\mathbf{r}-\mathbf{r}')\rho(\mathbf{r}')d\mathbf{r}'. \tag{8}$$

As a consequence, defining r_{max} as the distance beyond which the parabolic expansion [Eq. (6)] ceases to be valid, the corrective potential v^{corr} can be considered as nearly

parabolic, provided that the spread of the distribution is tolerably lower than $r_{\max}$.

C. Connection with existing schemes

Having justified the general characteristics of the electrostatic-potential correction, we now determine the terms in the expansion of v_0^{corr} [Eq. (6)]. The potential at the origin $v_0^{\text{corr}}(0)$ can be written in terms of the Madelung constant α_0 (Ref. 23) of a cubic lattice of point charges in a compensating jellium background,

$$v_0^{\text{corr}}(0) = \frac{\alpha_0}{L}. \tag{9}$$

(The calculation of the Madelung constant of a jellium-neutralized assembly of point charges is discussed in Appendix A.) Note that $v_0^{\text{corr}}(0)$ is positive, reflecting the stabilizing contribution from the jellium compensation. The value of $\nabla^2 v_0^{\text{corr}}(0)$ is then determined from Eq. (5),

$$\nabla^2 v_0^{\text{corr}}(0) = -\frac{4\pi}{L^3}. \tag{10}$$

Hence, the point-charge correction in the case of a cubic lattice can be expanded as

$$v_0^{\text{corr}}(\mathbf{r}) = \frac{\alpha_0}{L} - \frac{2\pi}{3L^3} r^2 + O(|\mathbf{r}|^4). \tag{11}$$

The terms in this parabolic expansion bear a strong resemblance to those entering into the Makov–Payne correction.[5] This correspondence is discussed further in Sec. II D.

The above expansion allows us to approximate the electrostatic correction induced by a set of compensating charges. Indeed, by introducing N charges, we can define a parabolic point-countercharge (PCC) potential $v_{\text{PCC}}^{\text{corr}}$ as

$$v_{\text{PCC}}^{\text{corr}}(\mathbf{r}) = \sum_{n=1}^{N} q_n \left(\frac{\alpha_0}{L} - \frac{2\pi}{3L^3} (\mathbf{r} - \mathbf{r}_n)^2 \right). \tag{12}$$

This expression may be rewritten as

$$v_{\text{PCC}}^{\text{corr}}(\mathbf{r}) = \frac{\alpha_0 q}{L} - \frac{2\pi q}{3L^3} r^2 + \frac{4\pi}{3L^3} \mathbf{p} \cdot \mathbf{r} - \frac{2\pi Q}{3L^3}, \tag{13}$$

where $q = \Sigma_n q_n$ is the total charge, $\mathbf{p} = \Sigma_n q_n \mathbf{r}_n$ denotes the total dipole moment, and $Q = \Sigma_n q_n r_n^2$ stands for the total quadrupole moment of the countercharge distribution. Equation (13) indicates that parabolic PCC schemes can correct periodic-image errors up to quadrupole-moment order. Note that no more than $N_{\max} = 7$ countercharges are sufficient to obtain the most accurate parabolic correction (one charge for q, two for $\mathbf{p}$, and four for Q). To obtain higher-order PCC corrections, one would need to determine more terms in the expansion of the point-charge correction beyond the parabolic contributions. An example of a complete harmonic expansion can be found in Ref. 24.

An alternative approach is to employ countercharges whose corrective potential can be handily computed. A popular choice is to use Gaussian densities, as proposed by Blöchl.[13] By repeating the preceding analysis for a Gaussian density of charge $q = +e$, we can expand the Gaussian corrective potential $v_{\sigma,L}^{\text{corr}}$ as

$$v_{\sigma,L}^{\text{corr}} = \frac{\alpha_{\sigma/L}}{L} - \frac{2\pi}{3L^3} r^2 + O(|\mathbf{r}|^4), \tag{14}$$

where $\alpha_{\sigma/L}$ is the Madelung constant of an assembly of Gaussians of width σ immersed in a compensating jellium in a cubic cell of length L. It is more convenient, however, to write the corrective potential directly as

$$v_{\sigma,L}^{\text{corr}}(\mathbf{r}) = v_\sigma(\mathbf{r}) - v'_{\sigma,L}(\mathbf{r}) = \frac{\text{erf}(r/\sigma)}{r} - \frac{1}{L^3} \sum_{\mathbf{g} \neq \mathbf{0}} \frac{4\pi}{g^2} e^{-\sigma^2 g^2/4} e^{i\mathbf{g}\cdot\mathbf{r}}, \tag{15}$$

where v_σ is the electrostatic potential of an isolated Gaussian charge and $v'_{\sigma,L}$ is the potential corresponding to a periodically repeated Gaussian in a jellium background. The sum in the right-hand side of the equation converges very rapidly and can be calculated using FFT techniques. By superimposing N compensating charges, the Gaussian-countercharge (GCC) corrective potential $v_{\text{GCC}}^{\text{corr}}$ can be expressed as

$$v_{\text{GCC}}^{\text{corr}}(\mathbf{r}) = \sum_{n=1}^{N} q_n v_{\sigma,L}^{\text{corr}}(\mathbf{r} - \mathbf{r}_n). \tag{16}$$

This results in the following approximation for the open-boundary potential v:

$$v(\mathbf{r}) \approx v'(\mathbf{r}) + v_{\text{GCC}}^{\text{corr}}(\mathbf{r}). \tag{17}$$

We underscore that this scheme is equivalent to the Gaussian scheme introduced by Blöchl[13] and the LMCC method proposed by Schultz.[14] The equivalence with the LMCC approach [Eq. (3) in Ref. 14] can be established by recasting Eq. (17) as

$$v(\mathbf{r}) \approx [v'(\mathbf{r}) - v'_{\text{GCC}}(\mathbf{r})] + v_{\text{GCC}}(\mathbf{r}), \tag{18}$$

where $v_{\text{GCC}}(\mathbf{r}) = \Sigma q_n v_\sigma(\mathbf{r} - \mathbf{r}_n)$ is the electrostatic potential generated by the isolated countercharge distribution and $v'_{\text{GCC}}(\mathbf{r}) = \Sigma q_n v'_{\sigma,L}(\mathbf{r} - \mathbf{r}_n)$ denotes the periodic potential.

We are now in a position to compare the corrective potentials $v_{\text{PCC}}^{\text{corr}}$ and $v_{\text{GCC}}^{\text{corr}}$ with the potential v^{corr} obtained as the direct difference between the open-boundary potential and its periodic counterpart. For our comparative analysis, we refer to the exact corrective potential v^{corr} as the density-countercharge (DCC) potential. The DCC potential is obtained by evaluating the Coulomb integral defining v at each grid point in the unit cell. (A cheaper alternative to this procedure is presented in the next section.) The PCC, GCC, and DCC potentials for a charged pyridazine cation in a cubic cell of length $L = 15$ bohr are plotted in Fig. 4. The PCC and GCC corrections are computed up to the dipole order. First, it should be noted that the maximal energy of the PCC potential is slightly above its GCC counterpart, reflecting the fact that the Madelung energy of an array of point charges immersed in a jellium is higher than that of a jellium-neutralized array of Gaussian charges (cf. Appendix A). In addition, the maximal DCC energy is found to be approximately 0.05 Ry above $\alpha_0 q/L$, indicating that the dipole PCC and GCC corrections tend to underestimate the energy of the

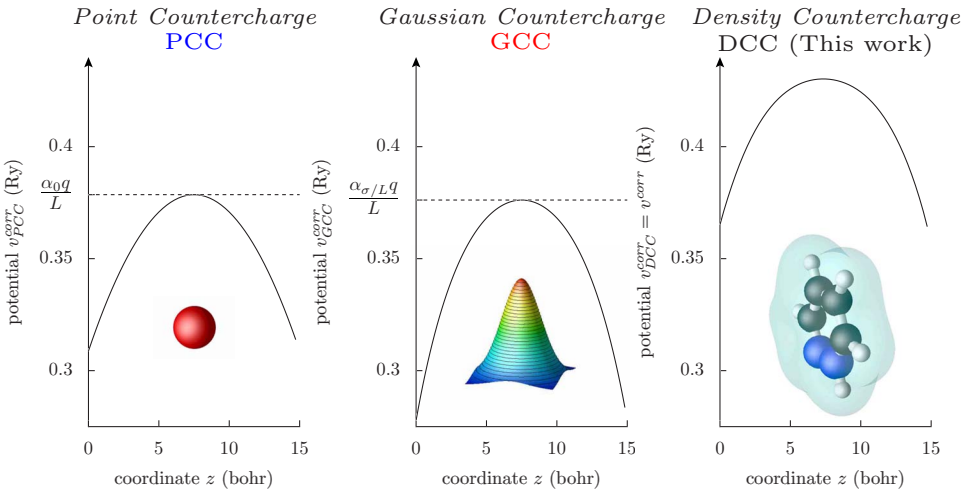

FIG. 4. (Color online) PCC (e.g., Makov–Payne), GCC (e.g., Blöchl and LMCC), and DCC corrective potentials for a pyridazine cation $C_4H_5N_2^+$ in a cubic cell of length $L=15$ bohr. The corrective potentials are plotted along the z axis perpendicular to the plane of the molecule, as defined in Fig. 1. The PCC and GCC corrections are calculated up to dipole order. The spread of the Gaussian countercharges is $\sigma=0.5$ bohr.

system. Moreover, the parabolic PCC potential is not as steep as its GCC counterpart, suggesting that the energy underestimation will be more significant for the GCC correction. Owing to the cubic symmetry of the cell, the PCC and GCC potentials display the same curvature in each direction of space, equal to one-third of $-4\pi\langle\rho\rangle$. In contrast, the curvature of the DCC potential is not uniform due to the nonspherical nature of the molecular charge density. This shape dependence suggests that the accuracy of the GCC correction could be improved by optimizing the geometry of the Gaussian countercharges.

In summary, we have shown that the PCC, GCC, and DCC approaches belong to the same class of periodic-image corrections. The analysis of the corrective potential has established that the parabolic PCC correction cannot eliminate periodic-image interactions beyond quadrupole order. Difficulties inherent in the GCC scheme have also been evidenced. To overcome these limitations, an efficient implementation of the DCC correction is presented in Sec. III.

D. Energy correction

To conclude this preliminary analysis, we give the expression of the energy correction ΔE^{corr} in terms of the corrective potential v^{corr}. The total electrostatic energy of the system is equal to

$$E = \frac{1}{2}\int v(\mathbf{r})\rho(\mathbf{r})d\mathbf{r}, \tag{19}$$

while the corrective energy can be expressed as[17]

$$\Delta E^{\text{corr}} = \frac{1}{2}\int v^{\text{corr}}(\mathbf{r})\rho(\mathbf{r})d\mathbf{r}. \tag{20}$$

It is worth mentioning that in the case of a single point countercharge $q=\int\rho(\mathbf{r})d\mathbf{r}$, the PCC energy correction can be written as

$$\Delta E_0^{\text{corr}} = \frac{1}{2}\int q v_0^{\text{corr}}(\mathbf{r})\rho(\mathbf{r})d\mathbf{r} = \frac{\alpha_0 q^2}{2L} - \frac{\pi q Q}{3L^3}. \tag{21}$$

Here, the first term corresponds to the Madelung energy correction, as proposed by Leslie and Gillian.[4] Note that the second term (quadrupole correction) differs from that proposed by Makov and Payne[5] by a factor of 1/2. In order to probe the accuracy of the PCC energy correction, we consider the simple case of two interacting Gaussian charges. The dependence of the electrostatic energy with respect to cell size is depicted in Fig. 5. Figure 5 shows the superior performance of the PCC correction [curve (b)] in comparison with that proposed in Ref. 5 [curve (c)]: At a cell size of 25 bohr, the error in the electrostatic energy is larger than 0.1 Ry using the energy correction of Ref. 5, while it is lower than 0.03 Ry using that given by Eq. (21). This comparative analysis illustrates the improved accuracy of the present PCC correction.

III. IMPLEMENTATION OF THE DENSITY-COUNTERCHARGE CORRECTION

A. Density-countercharge algorithm

In the preceding section, the corrective potential v^{corr} was calculated directly by subtracting the periodic potential from

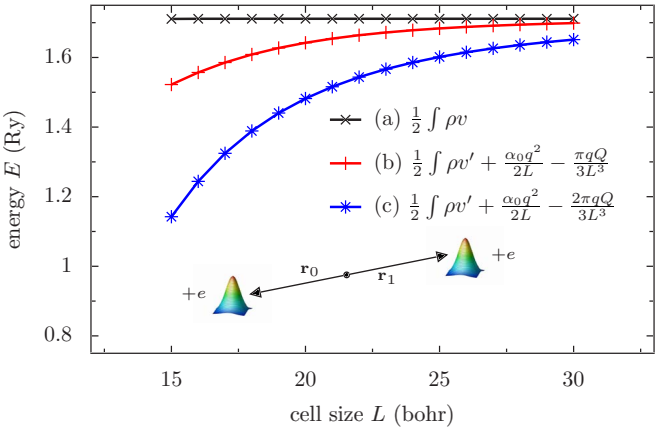

FIG. 5. (Color online) Electrostatic energy of two Gaussians of unit charge and unit spread calculated via (a) real-space integration, (b) reciprocal-space integration with the PCC energy correction given by Eq. (21), and (c) reciprocal-space integration with the energy correction given by Eq. (15) in Ref. 5. The Gaussian charges are positioned at $\mathbf{r}_0=(-5,-5,-5)$ and $\mathbf{r}_1=(5,5,5)$ (corresponding to a quadrupole moment Q of 153 a.u.).

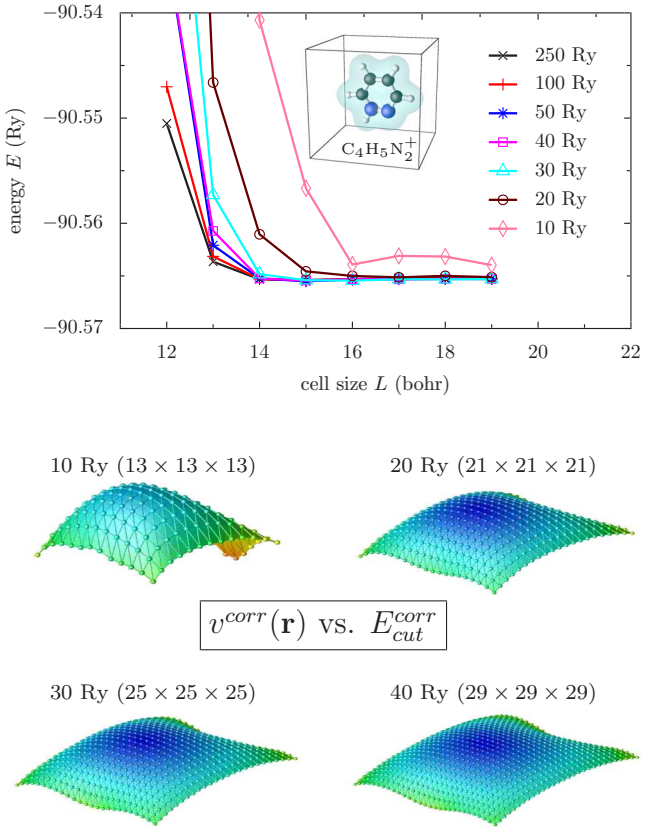

FIG. 6. (Color online) DCC total energy as a function of cell size for a pyridazine cation varying the coarse-grid cutoff $E_{\text{cut}}^{\text{corr}}$ from 10 Ry ($M=13\times13\times13$) to 250 Ry ($M=N=73\times73\times73$). Also depicted is the corrective potential v^{corr} in the plane of the molecule as a function of the coarse-grid resolution at a cell size of 15 bohr.

its open-boundary counterpart. The computational cost of this direct method is prohibitively high, on the order of $O(N^2)$ (where N is the number of grid points), corresponding to the evaluation of Coulomb integrals at each point of the grid. In this section, we present a scheme that reduces this computational burden. The scheme exploits both the Poisson equation for v^{corr} [Eq. (5)] and the fact that v^{corr} is smoothly varying.

First, we note that by taking into account appropriate boundary conditions, Eq. (5) can be solved efficiently using multigrid solvers.[25–30] Multigrid algorithms typically scale as $O(N \log N)$, that is, comparable to the scaling of an FFT computation. Hence, the overall cost of the calculation can be reduced from $O(N^2)$ to $O(N^{5/3})$, corresponding to the expense arising from the determination of the boundary conditions. Although a similar approach may be employed to directly solve the electrostatic equation defining v [Eq. (1)], we emphasize that Eq. (5) allows a considerable reduction in numerical error in the finite-difference evaluation of the electronic Laplacian.

By further exploiting this idea, it is possible to solve Eq. (5) on a grid much coarser than that used to discretize the charge density. To illustrate this fact, we consider a pyridazine cation in a periodic cubic cell of varied sizes (Fig. 6). The total energy of the system is calculated using density-functional theory.[31] An energy cutoff $E_{\text{cut}}=250$ Ry is applied to the plane-wave expansion of the charge density. The total energies are corrected using the DCC scheme by solving the electrostatic equation of v^{corr} on a coarse grid for several values of the energy cutoff denoted by $E_{\text{cut}}^{\text{corr}}$. By reducing the energy cutoff $E_{\text{cut}}^{\text{corr}}$ from 250 to 40 Ry, the corrected energies are observed to depart by less than 5×10^{-3} Ry from their converged values for cell sizes greater than 13 bohr. The ability to decrease the number of grid points without a significant loss of accuracy enables a substantial reduction in the additional computational cost from $O(N^{5/3})$ to $O(M^{5/3})$, where M is the number of coarse-grid points. Note that diminishing the plane-wave energy cutoff from 250 to 40 Ry at $L=15$ bohr reduces the cost of boundary-condition calculation by a factor of $29^5/73^5\approx1/100$.

Before presenting the algorithm, we draw attention to the fact that the DCC scheme relies on the central idea that most of the structural characteristics of the open-boundary potential v can be removed by subtracting its periodic counterpart v'. The residual v^{corr} (that is, the amount by which v' fails to reproduce v) is smooth and can be determined on a coarse grid at low computational cost. Additional computational savings come from the ability to avoid updating the potential v^{corr} at each step of the self-consistent-field (SCF) calculation, but instead at fixed interval between electronic iterations.

The DCC algorithm for a typical electronic-structure calculation can be described as follows. Let N^{corr} denote the number of SCF steps between each update of the corrective potential.

(1) Start from an initial charge distribution ρ on the fine grid.
(2) Calculate the periodic potential v' corresponding to ρ.
(3) Transfer ρ and v' on the coarse grid (tricubic interpolation[32]) to obtain the coarse-grid density $\tilde{\rho}$ and coarse-grid periodic potential $\tilde{v}'$.
(4) Calculate the real-space potential $\tilde{v}$ at the boundaries of the coarse grid from $\tilde{\rho}$ to obtain the Dirichlet boundary conditions $\tilde{v}^{\text{corr}}=\tilde{v}-\tilde{v}'$.
(5) Solve $\nabla^2\tilde{v}^{\text{corr}}=-4\pi\langle\rho\rangle$ (multigrid techniques) to obtain the corrective potential $\tilde{v}^{\text{corr}}$.
(6) Transfer $\tilde{v}^{\text{corr}}$ on the fine grid (tricubic interpolation) to obtain v^{corr} and calculate $v=v^{\text{corr}}+v'$.
(7) Perform N^{corr} electronic SCF steps.
(8) Iterate steps 2–7 until SCF convergence is reached.

Note that we employ real-space tricubic interpolation techniques in order to avoid oscillatory distortions inherent in Fourier transform interpolation schemes. We also underscore that the DCC algorithm can be efficiently parallelized since its most expensive step (namely, the calculation of the Dirichlet boundary conditions) scales linearly with the number of processors.

The above procedure can be adapted to one- and two-dimensional systems by considering the linear or planar average of the charge density for calculating the corrective potential.[16] (The validity of the linear- or planar-average approximations will be discussed in the last section.) The computational cost of this approach is moderate, on the order of $O(M^{1/3})$ and $O(M)$ for one and two dimensions, respectively.

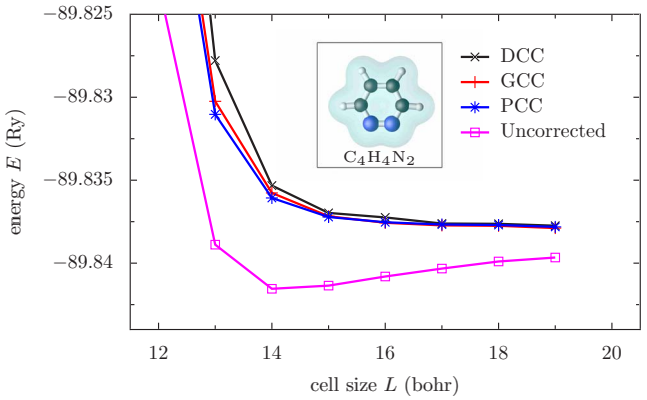

FIG. 7. (Color online) Total energy as a function of cell size for a neutral pyridazine molecule without correction and corrected using the PCC, GCC, and DCC schemes. The PCC and GCC corrections are calculated up to quadrupole order. The inset shows a pyridazine molecule in a cell of size $L=15$ bohr.

It should also be mentioned that the DCC algorithm can be used in combination with multipole-expansion methods for a rapid evaluation of the Dirichlet boundary conditions (step 4). The accuracy of this approach depends on the precision of the multipole expansion at the boundary of the supercell. (Section 3.4 of Greengard's dissertation[33] presents an analysis of the long-range accuracy of multipole expansions.) The performance of the multipole-expansion approach is reported in Appendix B.

B. Applications

The energy of a pyridazine molecule as a function of cell size L for each countercharge correction is reported in Fig. 7. For this neutral species, the uncorrected energy shows a characteristic minimum at $L=14$ bohr before slowly approaching its asymptotic value. In contrast, the corrected energies converge rapidly. We emphasize that all corrective schemes yield the same asymptotic energy (within less than 10^{-4} Ry). Although the three schemes demonstrate comparable convergence, it should be noted that the PCC method is slightly more accurate. In addition to further validating the energy expansion given by Eq. (21), this comparison suggests that the PCC correction can be preferred for studying neutral species—with the notable exception of elongated systems (e.g., polymer fragments or terminated nanotubes) for which the DCC method would be more accurate.

We now consider the energy of a pyridazine cation as a function of cell size (Fig. 8). We use energy cutoffs of 35 and 250 Ry for expanding the wave functions and the charge density, and select a coarse-grid cutoff of 35 Ry for calculating the DCC correction. Expectedly, the uncorrected energy converges very slowly with respect to L (at 19 bohr, the energy error is still larger than 0.15 Ry). The PCC and GCC corrections substantially improve the convergence of the total energy; reducing periodic-image errors by 1 order of magnitude. Using the DCC scheme, the energy is observed to converge even more rapidly, reflecting the exponential disappearance of energy errors arising from the charge density spilling across periodic cells: At a cell size of 15 bohr, which

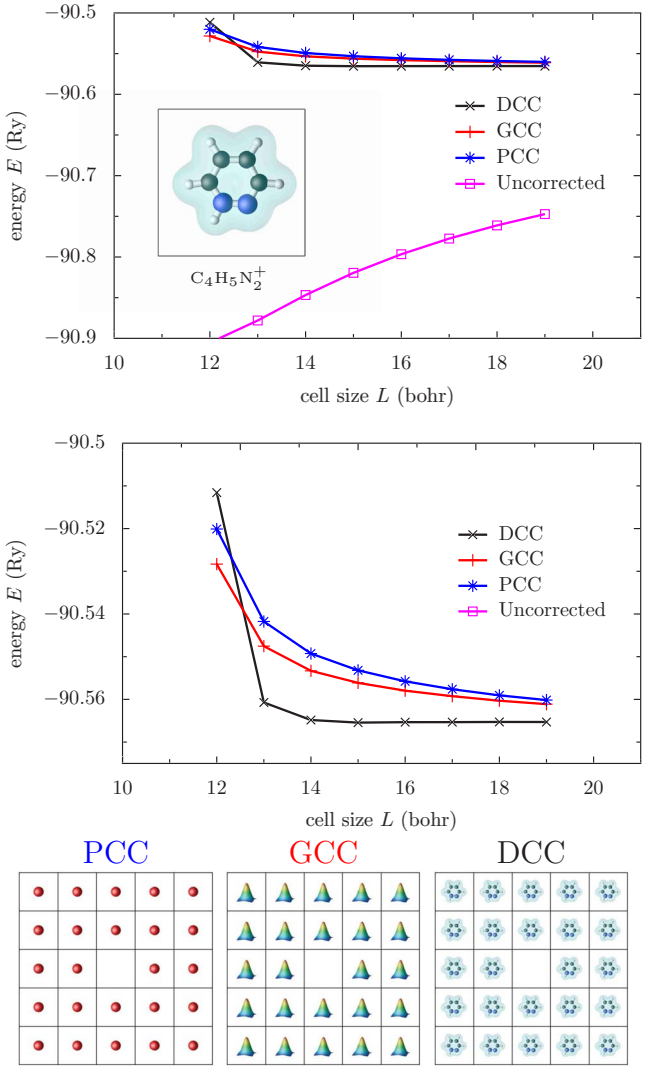

FIG. 8. (Color online) Total energy as a function of cell size for a pyridazine cation without correction and corrected using the PCC, GCC, and DCC schemes. The PCC and GCC corrections are calculated up to quadrupole order. The inset of the top graph shows a pyridazine cation in a cell of size $L=15$ bohr.

is barely larger than the size of the molecule, the DCC energy is converged within 10^{-4} Ry. The performance of each scheme as a function of the total computational time is shown on a logarithmic energy scale in Fig. 9. Each curve corresponds to cell sizes in the range of 12–19 bohr. In assessing the error ΔE, the converged energy was taken to be that calculated at a cell size of 25 bohr using the DCC correction. For a meaningful comparison with the DCC scheme, the PCC and GCC corrective potentials are also updated at fixed SCF intervals. We observe that the computational cost of the corrected calculations is comparable to that without correction for a considerable improvement in accuracy. For this charged system, the DCC approach constitutes the most advantageous alternative; improving the energy precision by 2 orders of magnitude over the PCC and GCC corrections for cell sizes above 15 bohr.

The performance of the DCC and GCC corrective schemes for a neutral polyvinylidene fluoride (PVDF) chain

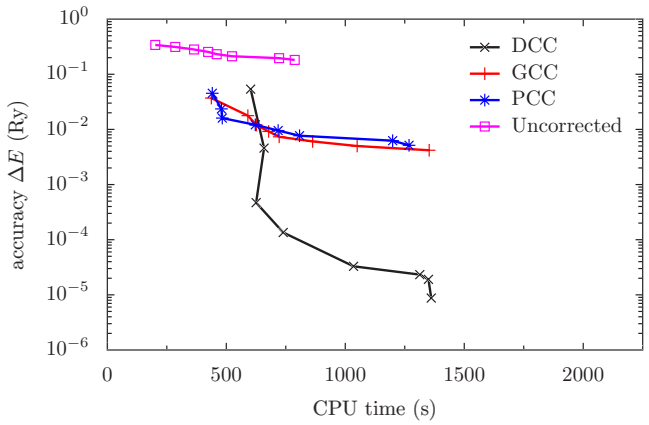

FIG. 9. (Color online) Accuracy of the total energy as a function of computational time without correction and using the PCC, GCC, and DCC schemes for cell sizes in the range of 12–19 bohr. For each scheme, the corrective potential is updated every five SCF iterations.

is reported in Fig. 10. The comparison shows a significant improvement in energy convergence for both schemes. As shown in the inset of Fig. 10, the performance of the DCC scheme is perceptibly superior to that of the GCC scheme. We emphasize that for systems exhibiting one-dimensional periodicity, the additional computational cost due to the electrostatic correction is moderate, on the order of $O(M)$ at most.

The DCC scheme can also be used in the calculation of work functions as it solves energy-reference issues by automatically setting the vacuum level to zero. Figure 11 depicts the convergence of the opposite Fermi energy of a Pt(100) slab as a function of transverse cell size. The wave function, charge-density, and corrective potential energy cutoffs are 25, 200, and 150 Ry, respectively. We use a shifted $5\times5\times1$ mesh with a cold-smearing occupation function[34] (smearing temperature of 0.03 Ry) to sample the Brillouin zone. Without correction, the relative error in the Fermi energy stays above 100% for all cell sizes in the considered range. Using the GCC scheme, the convergence of the Fermi level improves greatly: At 150 bohr, the relative error decreases to approximately 0.1 eV. By employing the DCC corrective scheme, the calculated Fermi energy is converged within 2 meV at 60 bohr and 0.1 meV at 150 bohr. Thus, the DCC scheme allows us to directly determine the work function of a metal as the opposite of the calculated Fermi energy using supercells of minimal size. A similar convergence improvement is obtained for the work function of carbon nanotubes.[35] Besides improving the convergence of total energies, the DCC approach can be employed to correct structural and vibrational properties[11] and to calculate linear response characteristics with a reduced computational effort.[11,12,36]

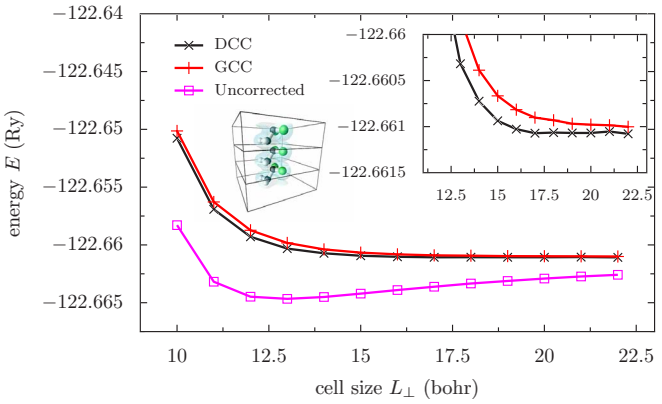

FIG. 10. (Color online) Total energy as a function of transverse cell size for a PVDF chain without correction and using the GCC and DCC schemes.

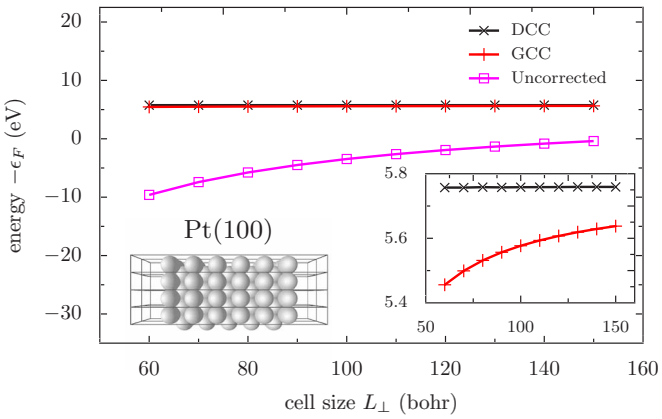

FIG. 11. (Color online) Convergence of the opposite Fermi energy $-\epsilon_F$ as a function of transverse cell size for a Pt(100) slab without correction and using the GCC and DCC schemes.

IV. BEYOND THE LINEAR- AND PLANAR-AVERAGE APPROXIMATIONS

A. Treating systems with partial periodicity

In the preceding sections, we have assumed that the corrective potential of a one- or two-dimensional system can be obtained by homogenizing the system along its periodicity directions, as initially proposed by Baldereschi *et al.*[16] This approach, referred to as the linear- or planar-average approximation, has been frequently employed in electronic-structure calculations.[15–17,20,37]

Alternative schemes adapting the Ewald method to evaluate conditionally convergent lattice sums[38] or generalizing the fast multiple method (FMM) approach[39,40] have also been proposed for systems exhibiting partial periodicity. Such schemes are particularly suited to localized-orbital calculations but are of relatively limited applicability for plane-wave implementations. Here, we propose an efficient method to calculate the electrostatic potential for partially periodic systems, taking into account the full three-dimensional structure of the charge distribution. In addition to presenting this methodological extension, we discuss how to assess the validity of the linear- and planar-average approximations *a priori* in terms of structural characteristics of the system.

B. Density-countercharge scheme for one-dimensional periodicity

To introduce the DCC approach for one-dimensional systems, we first study the electrostatic problem corresponding to an isolated sinusoidal-density line,

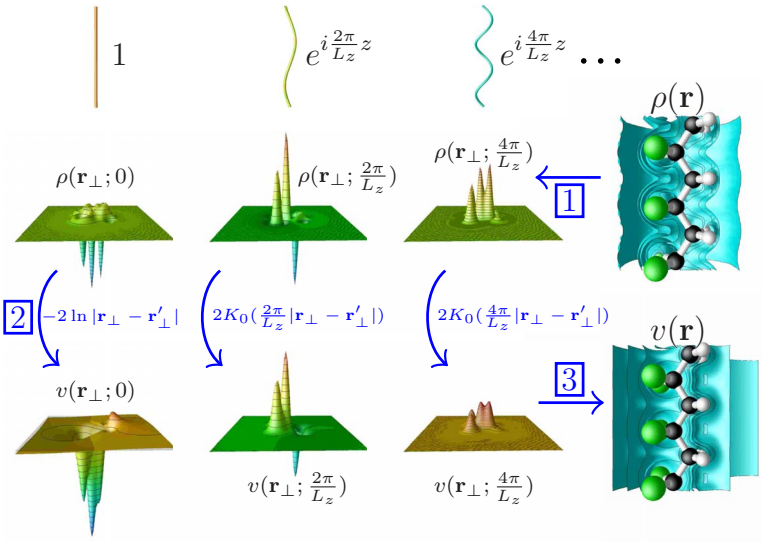

FIG. 12. (Color online) Fourier-decomposition calculation of the electrostatic potential $v(\mathbf{r}_\perp,z)=\Sigma_{g_z}v(\mathbf{r}_\perp;g_z)e^{ig_zz}$ for an infinite PVDF chain. (1) The longitudinal Fourier transform of the charge density is calculated to obtain the contributions from each axial wave vector g_z. (2) The electrostatic potential generated by each Fourier component of the charge density is calculated using the Green's functions. (3) The electrostatic potential is then transformed back to real space.

$$\rho(\mathbf{r}) = \delta^{(2)}(\mathbf{r}_\perp)\exp(ig_zz), \tag{22}$$

where $\delta^{(2)}$ stands for the two-dimensional Dirac delta function and $\mathbf{r}_\perp$ denotes the transverse coordinates (x,y). By making the ansatz $v(\mathbf{r})=\mathcal{G}(\mathbf{r}_\perp;g_z)\exp(ig_zz)$ for the Green's function, we obtain the following:

$$(\nabla_\perp^2 - g_z^2)\mathcal{G}(\mathbf{r}_\perp;g_z) = -4\pi\delta^{(2)}(\mathbf{r}_\perp). \tag{23}$$

The solution of this generalized electrostatic problem can be written as

$$\mathcal{G}(\mathbf{r}_\perp;0) = -2\ln|\mathbf{r}_\perp|,$$

$$\mathcal{G}(\mathbf{r}_\perp;g_z) = 2K_0(g_z|r_\perp|) \quad \text{for } g_z \neq 0, \tag{24}$$

where K_0 is the modified Bessel function of the second kind. Note that $K_0(g_z|\mathbf{r}_\perp|)=-\ln|\mathbf{r}_\perp|+\cdots$ when $g_z|\mathbf{r}_\perp|$ approaches zero, reflecting the fact that a sinusoidal-density line can be considered as uniform when seen from a distance much smaller than its wavelength. The potential of an arbitrary one-dimensional charge distribution can be analytically determined by knowing the electrostatic potential generated by a single line, as illustrated in Fig. 12. The general procedure consists of calculating the one-dimensional Fourier transform of ρ to obtain its longitudinal Fourier components $\rho(\mathbf{r}_\perp;g_z)$ (step 1). Each individual component is then convoluted with the electrostatic potential generated by a sinusoidal density, as expressed in Eq. (24), to obtain the Fourier components $v(\mathbf{r}_\perp;g_z)$ of the open-boundary potential (step 2),

$$v(\mathbf{r}_\perp;0) = -2\int \ln|\mathbf{r}_\perp-\mathbf{r}'_\perp|\rho(\mathbf{r}'_\perp;0)d\mathbf{r}'_\perp,$$

$$v(\mathbf{r}_\perp;g_z) = 2\int K_0(g_z|\mathbf{r}_\perp-\mathbf{r}'_\perp|)\rho(\mathbf{r}'_\perp;g_z)d\mathbf{r}'_\perp \quad \text{for } g_z \neq 0. \tag{25}$$

Finally, the open-boundary potential is transformed back to real space (step 3). We underscore that this procedure directly extends the linear-average approximation since the linear average of the charge density corresponds to the first term of the one-dimensional Fourier decomposition. Thus, averaging the charge density along the axis of periodicity amounts to restricting the Fourier series to its $g_z=0$ term.

To estimate errors resulting from this truncation, we analyze the asymptotic behavior of $v(\mathbf{r}_\perp;g_z\neq0)$ at large $g_z|\mathbf{r}_\perp|$ as

$$v(\mathbf{r}_\perp;g_z) = O\left(\frac{e^{-g_z|\mathbf{r}_\perp|}}{\sqrt{g_z|\mathbf{r}_\perp|}}\right) \quad \text{when } g_z|\mathbf{r}_\perp| \gg 1. \tag{26}$$

From Eq. (26), the validity of the linear average approach can be assessed by calculating the ratio of the cell size in the transverse direction $L_\perp$ (that is, the distance between periodic replicas) to the typical wavelength $\lambda_\parallel$ characterizing longitudinal inhomogeneities in the system. For large values of the dimensionless parameter $L_\perp/\lambda_\parallel$, periodic-image interactions are predominantly due to the logarithmic first-order contribution $v(\mathbf{r}_\perp;0)$ corresponding to the linear average of the charge density. Thus, as expected intuitively, the linear-average approximation is valid in this situation. In contrast, when $\lambda_\parallel$ is comparable to the distance $L_\perp$ between the periodic images, higher-order Fourier components $v(\mathbf{r}_\perp;g_z)$ corresponding to $g_z\approx2\pi/\lambda_\parallel$ must also be taken into consideration.

Despite its merit in discussing the validity of the linear-average approximation, determining the open-boundary potential using the preceding approach requires expensive summations for each point $\mathbf{r}_\perp$ of the two-dimensional grid and for each longitudinal wave vector g_z. Along the same methodological lines as those of the DCC algorithm, a substantial reduction of computational cost can be achieved by exploiting the periodic potential v', whose longitudinal Fourier components can be computed inexpensively using FFT techniques, as follows:

$$v'(\mathbf{r}_\perp;0) = \sum_{\mathbf{g}_\perp\neq\mathbf{0}} \frac{4\pi}{\mathbf{g}_\perp^2}\rho(\mathbf{g}_\perp)e^{i\mathbf{g}_\perp\cdot\mathbf{r}_\perp},$$

$$v'(\mathbf{r}_\perp;g_z)=\sum_{\mathbf{g}_\perp}\frac{4\pi}{\mathbf{g}_\perp^2+g_z^2}\rho(\mathbf{g}_\perp+g_z\hat{\mathbf{z}})e^{i\mathbf{g}_\perp\cdot\mathbf{r}_\perp}\quad\text{for}\quad g_z\neq 0. \tag{27}$$

After coarse-grid interpolation, the component of the open-boundary potential $v(\mathbf{r}_\perp;g_z)$ can be calculated at the boundaries of the domain, yielding Dirichlet boundary conditions for the smooth corrective components $v^{\text{corr}}(\mathbf{r}_\perp;g_z)=v(\mathbf{r}_\perp;g_z)-v'(\mathbf{r}_\perp;g_z)$. The corresponding g_z-dependent electrostatic problems read as

$$\nabla^2 v^{\text{corr}}(\mathbf{r}_\perp;0)=-4\pi\langle\rho\rangle,$$

$$(\nabla^2-g_z^2)v^{\text{corr}}(\mathbf{r}_\perp;g_z)=0\quad\text{for}\quad g_z\neq 0. \tag{28}$$

These differential equations can be solved by using efficient multigrid techniques. Once calculated, the longitudinal Fourier components of the electrostatic correction are added to those of the periodic potential, thereby recovering $v(\mathbf{r}_\perp;g_z)$. Finally, the potential $v(\mathbf{r})$ is computed via an inverse Fourier transform.

C. Density-countercharge scheme for two-dimensional periodicity

The electrostatic potential of a slab can be calculated in real space using a scheme analogous to that presented above. A similar Green's function formalism for two-dimensional systems is developed in Refs. 41 and 42. The prescription consists in performing two-dimensional Fourier transforms to obtain the charge-density profile $\rho(z;\mathbf{g}_\parallel)$ associated with each wave vector $\mathbf{g}_\parallel=(g_x,g_y)$ parallel to the surface. Solving the electrostatic problem for sinusoidal-density layers, the two-dimensional Green's functions $\mathcal{G}(z;\mathbf{g}_\parallel)$ can be written as

$$\mathcal{G}(z;\mathbf{0})=-2\pi|z|,$$

$$\mathcal{G}(z;\mathbf{g}_\parallel)=2\pi\frac{e^{-g_\parallel|z|}}{g_\parallel}\quad\text{for}\quad g_\parallel\neq 0. \tag{29}$$

Hence, as in the one-dimensional case, the density-average approximation is valid provided that the geometrical parameter $L_\perp/\lambda_\parallel$ is large—this criterion is identical to that derived by Natan *et al.*[19] In addition, the above expressions allow one to determine the corrective potential of a two-dimensional system by integrating the differential equations,

$$\frac{d^2}{dz^2}v^{\text{corr}}(z;\mathbf{0})=-4\pi\langle\rho\rangle,$$

$$\left(\frac{d^2}{dz^2}-g_\parallel^2\right)v^{\text{corr}}(z;\mathbf{g}_\parallel)=0\quad\text{for}\quad g_\parallel\neq 0. \tag{30}$$

Parenthetically, it should be noted that Eq. (30) can be solved analytically by taking into account the boundary conditions calculated by superposition—that is, by convoluting the longitudinal components of $\mathcal{G}$ and ρ [similar to Eq. (25)], then subtracting out the components of v'. Therefore, the additional cost of the two-dimensional DCC correction is negligible.

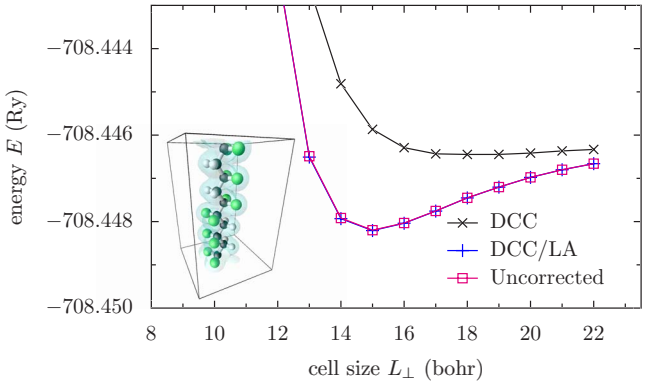

FIG. 13. (Color online) Total energy as a function of transverse cell size for a $-[CH_2CF_2]_3-[CF_2CH_2]_3-$ polymer chain without correction, corrected using the density-countercharge scheme with full Fourier decomposition (DCC) and by limiting the density-countercharge decomposition to the linear-average $\mathbf{g}=0$ component (DCC/LA).

D. Applications

The convergence of the total energy with respect to transverse cell size for a fluoropolymer chain $-[CH_2CF_2]_3-[CF_2CH_2]_3-$ of long periodicity $\lambda_\parallel\approx 24$ bohr is depicted in Fig. 13. We employ ultrasoft pseudopotentials[43] with energy cutoffs of 50 and 500 Ry for the plane-wave expansions of the electronic wave function and charge density, respectively. The energy cutoff for calculating the corrective potential is 80 Ry. We use a shifted $1\times 1\times 2$ mesh with cold-smearing occupations[34] (smearing temperature of 0.02 Ry). Within the linear-average approximation (DCC/LA), the corrected energy closely coincides with the uncorrected energy due to the absence of polarization in the longitudinal average of the charge density. For the cell parameters considered, the geometrical ratio $L_\perp/\lambda_\parallel$ varies from 0.5 to 0.9, that is, beyond the range of validity of the linear-average approximation. As a result, we observe that the DCC/LA energy slowly converges toward its asymptotic value. In contrast, the DCC scheme with full Fourier decomposition significantly improves the convergence of the total energy (at 16 bohr, the accuracy of DCC energy is approximately 5×10^{-5} Ry, whereas that of the uncorrected and DCC/LA energies is approximately 10^{-3} Ry). Figure 14 depicts the convergence of the force on one of the fluorine atoms. Similar to the convergence of the total energy, the atomic-force convergence is seen to substantially improve by applying the DCC correction: At 16 bohr, the DCC force is converged within less than 10^{-4} Ry/bohr, while that obtained without correction or using the DCC/LA scheme is converged within 10^{-3} Ry/bohr. We underscore that the computational cost of the DCC correction is moderate. Indeed, at 16 bohr, the additional cost is ~8%.

To conclude this study, we consider the electronic density response of a graphene sheet subject to a perturbation field. Figure 15 reports the dependence of the charge-density linear response function $\chi=\delta n/\delta v$ with respect to the interplane distance $L_\perp$ for a longitudinal sinusoidal perturbation of wave vector $g_\parallel=\frac{1}{25}$ bohr^{-1}. With a large wavelength of the

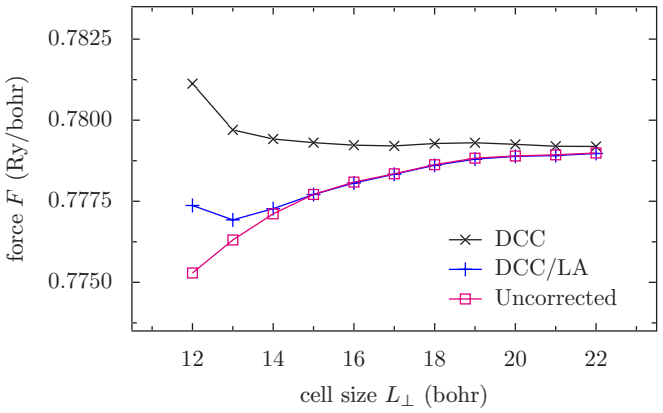

FIG. 14. (Color online) Force on one of the fluorine atoms along a transverse lattice direction as a function of transverse cell size for a $-[CH_2CF_2]_3-[CF_2CH_2]_3-$ polymer chain without correction, corrected using the density-countercharge scheme with full Fourier decomposing (DCC) and by limiting the density-countercharge decomposition to the linear-average $\mathbf{g}=0$ component (DCC/LA).

perturbation field ($\lambda_\parallel=157$ bohr), the uncorrected response coefficient does not converge until cell sizes on the order of hundreds of bohrs are reached. Contrary to uncorrected calculations, the DCC-corrected linear response rapidly converges with a negligible increase in computation cost. For comparison, at an interplane distance of $L_\perp=50$ bohr, the relative error in the uncorrected linear response is on the order of 25%, while it is lower than 1% using the DCC correction.

V. CONCLUSION

We have introduced the notion of a corrective potential for isolated systems, defined as the difference between the exact electrostatic potential (usually open boundary) and its periodic counterpart, and have studied its analytic properties in detail. Such a formulation has allowed us to more broadly frame well-established electrostatic correction schemes in periodic-boundary conditions, suggesting possible improvements and highlighting the incorrect expansion for the quadrupole term in the original Makov–Payne approach. Based on the analytic properties of the corrective potential, we have shown that periodic-image errors can be eliminated at a moderate computational cost of $O(M^{5/3})$, where M is the number of points of the mesh used in the calculation of the corrective potential, which is generally about 2 orders of magnitude smaller than the number of points of the charge-density grid. The resulting DCC scheme owes its improved efficiency to the rapid determination of the exact boundary conditions characterizing the electrostatic potential. By applying the DCC algorithm to large complex molecules and extended systems, we have shown that it allows the use of unit cells of minimal size and represents a beneficial compromise between cost and accuracy. We have also discussed the validity of the linear- and planar-average approximations routinely employed in the study of partially periodic systems. An efficient DCC scheme going beyond these conventional approximations for highly inhomogeneous low-dimensional systems has been proposed and validated.

Relevant applications for the DCC algorithm include the study of molecular adsorption at solid-vacuum interfaces in the constant-charge regime, the determination of structural parameters, the correction of vibrational spectra, the inexpensive calculation of work functions, and the determination of linear response properties with reduced computational effort.

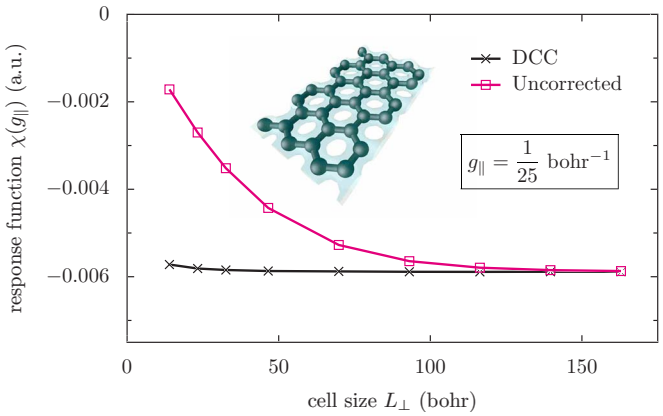

FIG. 15. (Color online) Charge-density linear response function $\chi(g_\parallel)$ as a function of transverse cell size for a graphene sheet without correction and corrected using the density-countercharge potential corresponding to $g_\parallel$ (DCC).

ACKNOWLEDGMENTS

The calculations in this work have been performed using the QUANTUM-ESPRESSO package[44] and the conjugate-gradient multigrid solver developed by Holst[45] as part of the parallel algebraic multigrid/finite-element toolkit. Both software packages are licensed for use under the GNU General Public License. The authors acknowledge support from the MURI Grant No. DAAD 19-03-1-0169, NSF-NIRT Grant No. DMR-0304019, and ISN-ARO Grant No. DAAD 19-02-D-0002. I.D. personally thanks the École Nationale des Ponts et Chaussées (France) and the Martin Family Society of Fellows for Sustainability for their help and support. Comments and suggestions from Jean-Luc Fattebert and Éric Cancès about the use of multigrid algorithms and from Raffaele Resta about electrostatics in periodic-boundary conditions are gratefully acknowledged. The authors thank Brandon Wood, Nicolas Poilvert, Young-Su Lee, Arash Mostofi, Oswaldo Dieguez, and Damian Scherlis for valuable comments and suggestions.

APPENDIX A: MADELUNG CONSTANTS AND GAUSSIAN POTENTIALS

In this appendix, we determine the Madelung constants of periodic point charges immersed in a compensating jellium background in one, two, and three dimensions for lattices characterized by a single geometric parameter L. A compilation of high-precision values for these fundamental constants is generally not found in the literature.

TABLE I. Madelung constants in one, two, and three dimensions computed using the procedure described in Appendix A along with the quantities used in the calculation. Ei denotes the exponential integral and $\gamma=0.577\ 215\ 665$ is the Euler constant.

3D lattice	α_0	2D lattice	α	1D lattice	α_0
Cubic	2.837297479	Squared	2.621065852	Linear	$-\pi/3$
Body-centered	3.639233449	Trigonal	2.786075893		
Face-centered	4.584862074				
$v_\sigma(r)=\frac{1}{r}\mathrm{erf}(\frac{r}{\sigma})$		$v_\sigma(r)=-\ln(\frac{r^2}{\sigma^2})+\mathrm{Ei}(-\frac{r^2}{\sigma^2})$		$v_\sigma(z)=-2\pi(z\mathrm{erf}(\frac{z}{\sigma})+\frac{\sigma}{\sqrt{\pi}}e^{-z^2/\sigma^2})$	
$v'_{\sigma,L}(r)=\frac{1}{V}\Sigma_{\mathbf{g}\neq\mathbf{0}}\frac{4\pi}{g^2}e^{-\sigma^2g^2/4+i\mathbf{g}\cdot\mathbf{r}}$		$v'_{\sigma,L}(r)=\frac{1}{S}\Sigma_{\mathbf{g}\neq\mathbf{0}}\frac{4\pi}{g^2}e^{-\sigma^2g^2/4+i\mathbf{g}\cdot\mathbf{r}}$		$v'_{\sigma,L}(z)=\frac{1}{L}\Sigma_{g\neq0}\frac{4\pi}{g^2}e^{-\sigma^2g^2/4+ig\cdot z}$	
$v_\sigma(0)=\frac{2}{\sqrt{\pi}\sigma}$		$v_\sigma(0)=\gamma$		$v_\sigma(0)=-2\sqrt{\pi}\sigma$	
$v'_{\sigma,L}(0)=\frac{2}{\sqrt{\pi}\sigma}-\frac{\alpha_0}{L}+\frac{\pi\sigma^2}{L^3}+\cdots$		$v'_{\sigma,L}(0)=\ln(\frac{L^2}{\sigma^2})-\alpha+\gamma+\frac{\pi\sigma^2}{L^2}+\cdots$		$v'_{\sigma,L}(0)=-L\alpha_0-2\sqrt{\pi}\sigma+\frac{\pi\sigma^2}{L}+\cdots$	
$\alpha_{\sigma/L}=\alpha_0-\frac{\pi\sigma^2}{L^2}+\cdots$		$\alpha_{\sigma/L}=-\ln(\frac{L^2}{\sigma^2})+\alpha-\frac{\pi\sigma^2}{L^2}+\cdots$		$\alpha_{\sigma/L}(0)=\alpha_0-\frac{\pi\sigma^2}{L^2}+\cdots$	

These values are computed using the asymptotic expansion of the Madelung constant $\alpha_{\sigma/L}$ of an array of Gaussian charges of spread σ in a compensating jellium, which is defined as

$$\alpha_{\sigma/L}=(v_\sigma(0)-v'_{\sigma,L}(0))L^{d-2}, \tag{A1}$$

where d is the spatial dimension. To obtain the expansion of $\alpha_{\sigma/L}$ in the limit $\sigma/L\to0$, we may write $v'_{\sigma,L}(0)$ as

$$v'_{\sigma,L}(0)=\frac{L^{2-d}}{\Omega_d}w_d\left(\frac{\sigma^2}{L^2}\right), \tag{A2}$$

$$w_d\left(\frac{\sigma^2}{L^2}\right)=\sum_{\mathbf{g}'\neq\mathbf{0}}\frac{4\pi}{g'^2}\exp\left(-\frac{g'^2}{4}\cdot\frac{\sigma^2}{L^2}\right), \tag{A3}$$

where Ω_d is the volume of d-dimensional unit cell and $\mathbf{g}'=L\mathbf{g}$ denotes the dimensionless wave vector. By differentiating w_d with respect to σ^2/L^2, we obtain

$$\frac{dw_d}{d(\sigma^2/L^2)}=-\pi\sum_{\mathbf{g}'\neq\mathbf{0}}\exp\left(-\frac{g'^2}{4}\cdot\frac{\sigma^2}{L^2}\right)$$

$$=\pi-\pi\sum_{\mathbf{g}'}\exp\left(-\frac{g'^2}{4}\cdot\frac{\sigma^2}{L^2}\right). \tag{A4}$$

In the limit $\sigma/L\to0$, this derivative becomes

$$\frac{dw_d}{d(\sigma^2/L^2)}=\pi-\frac{\Omega_d}{\pi^{d-1}}\left(\frac{\sigma^2}{L^2}\right)^{-d/2}\int_{R^d}e^{-u^2}d\mathbf{u}+\cdots. \tag{A5}$$

By integrating this expression, we obtain the asymptotic expansions of $v'_{\sigma,L}(0)$ and $\alpha_{\sigma/L}$ listed in Table I.

Hence, the Madelung constant α_0 can be calculated with high accuracy from the expansion of $\alpha_{\sigma/L}$. In the case of a cubic lattice of point charges, we obtain

$$\alpha_0\approx\alpha_{\sigma/L}+\frac{\pi\sigma^2}{L^2}-\sum_{\mathbf{n}\neq\mathbf{0}}\frac{1}{|\mathbf{n}|}\mathrm{erfc}\left(\frac{L}{\sigma}|\mathbf{n}|\right)$$

$$\approx\frac{1}{L^2}\sum_{\mathbf{g}\neq\mathbf{0}}\frac{4\pi}{g^2}e^{-\sigma^2g^2/4}-\frac{2L}{\sqrt{\pi}\sigma}$$

$$+\frac{\pi\sigma^2}{L^2}-\sum_{\mathbf{n}\neq\mathbf{0}}\frac{1}{|\mathbf{n}|}\mathrm{erfc}\left(\frac{L}{\sigma}|\mathbf{n}|\right), \tag{A6}$$

where $\mathbf{n}=(i,j,k)$ denotes an integer vector. Figure 16 illustrates the rapid convergence of the Madelung constant calculated from Eq. (A6) for a cubic cell. This expression converges considerably faster than the expression frequently found in the literature,

$$\alpha_0\approx\frac{1}{L^2}\sum_{\mathbf{g}\neq\mathbf{0}}\frac{4\pi}{g^2}e^{-\sigma^2g^2/4}-\frac{2L}{\sqrt{\pi}\sigma}-\sum_{\mathbf{n}\neq\mathbf{0}}\frac{1}{|\mathbf{n}|}\mathrm{erfc}\left(\frac{L}{\sigma}|\mathbf{n}|\right). \tag{A7}$$

Although a similar procedure can be applied without additional difficulty for any dimensionality, we draw attention to the fact that in two dimensions, $\alpha_{\sigma/L}$ is not equal to the Madelung constant α in the limit $\sigma/L\to0$ due to the logarithmic divergence of the potential. For a more complete discussion of the two-dimensional case, we refer the reader to the study of Cichocki and Felderhof.[24] As a final remark, we note that the one-dimensional Madelung constant can be analytically determined from the relation

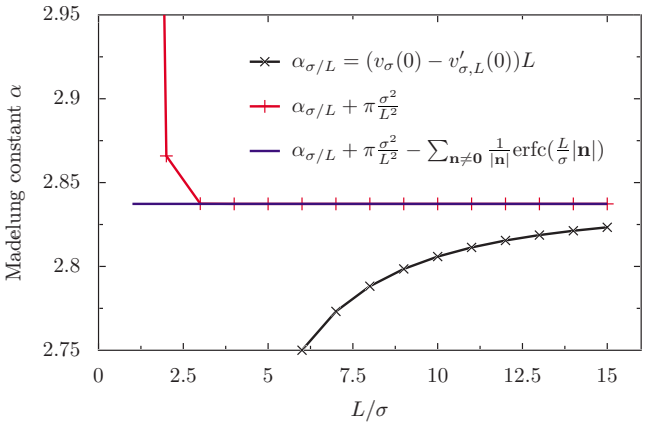

FIG. 16. (Color online) Convergence of the Madelung constant as a function of the geometric parameter L/σ for a cubic unit cell using the approximation given by Eq. (A6). [The black curve is Eq. (A6) without the $\pi\sigma^2/L^2$ and the complementary-error-function terms, the red curve is Eq. (A6) without the complementary-error-function term, and the blue curve is Eq. (A6)]. Note the negligible contribution of the complementary-error-function term beyond $L/\sigma=3$ and the improvement in convergence brought about by the term $\pi\sigma^2/L^2$.

$$\sum_{n=1}^{+\infty} \frac{1}{n^2} = \frac{\pi^2}{6}. \tag{A8}$$

APPENDIX B: PERFORMANCE OF THE MULTIPOLE-EXPANSION METHOD

The performance of the multipole-expansion adaptation of the DCC scheme—the multipole-countercharge (MCC) correction—for a pyridazine cation is compared to that of the PCC and GCC schemes in Fig. 17. The size of the calculation cell ranges from 12 to 19 bohr. The parameters used in these calculations are those detailed in Sec. III B. Note the good performance of the MCC approach, which improves the energy accuracy by almost 1 order of magnitude in comparison with the PCC and GCC schemes for cell sizes above 17 bohr.

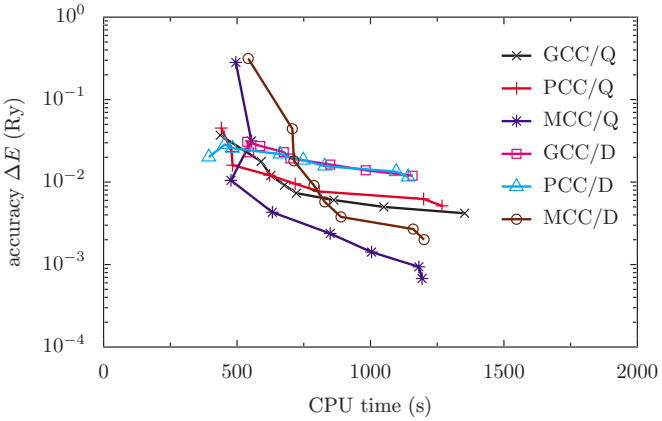

FIG. 17. (Color online) Accuracy of the total energy of a pyridazine cation as a function of computational time using the PCC, GCC, and MCC schemes for cell sizes in the range of 12–19 bohr. The labels *D* (dipole) and *Q* (quadrupole) indicate the order of the multipole expansion. For each scheme, the corrective potential is updated every five SCF iterations.

*dabo_is@mit.edu

[1] M. Frigo and S. G. Johnson, Proc. IEEE **93**, 216 (2005).
[2] J. W. Cooley and J. W. Tukey, Math. Comput. **19**, 297 (1965).
[3] M. T. Heideman, D. H. Johnson, and C. S. Burrus, Arch. Hist. Exact Sci. **34**, 265 (1985).
[4] M. Leslie and N. J. Gillian, J. Phys. C **18**, 973 (1985).
[5] G. Makov and M. C. Payne, Phys. Rev. B **51**, 4014 (1995).
[6] R. N. Barnett and U. Landman, Phys. Rev. B **48**, 2081 (1993).
[7] D. Marx, J. Hutter, and M. Parrinello, Chem. Phys. Lett. **241**, 457 (1995).
[8] D. Marx and J. Hutter, *Modern Methods and Algorithms of Quantum Chemistry*, 2nd ed. (Forschungszentrum Jülich, Germany, 2000), pp. 329–477.
[9] G. J. Martyna and M. E. Tuckerman, J. Chem. Phys. **110**, 2810 (1999).
[10] M. R. Jarvis, I. D. White, R. W. Godby, and M. C. Payne, Phys. Rev. B **56**, 14972 (1997).
[11] C. A. Rozzi, D. Varsano, A. Marini, E. K. U. Gross, and A. Rubio, Phys. Rev. B **73**, 205119 (2006).
[12] S. Ismail-Beigi, Phys. Rev. B **73**, 233103 (2006).
[13] P. E. Blöchl, J. Chem. Phys. **103**, 7422 (1995).
[14] P. A. Schultz, Phys. Rev. Lett. **84**, 1942 (2000).
[15] J. Neugebauer and M. Scheffler, Phys. Rev. B **46**, 16067 (1992).
[16] A. Baldereschi, S. Baroni, and R. Resta, Phys. Rev. Lett. **61**, 734 (1988).
[17] L. Bengtsson, Phys. Rev. B **59**, 12301 (1999).
[18] B. Meyer and D. Vanderbilt, Phys. Rev. B **63**, 205426 (2001).
[19] A. Natan, L. Kronik, and Y. Shapira, Appl. Surf. Sci. **252**, 7608 (2006).
[20] A. Y. Lozovoi and A. Alavi, Phys. Rev. B **68**, 245416 (2003).
[21] I. Souza, J. Ìñiguez, and D. Vanderbilt, Phys. Rev. Lett. **89**, 117602 (2002).
[22] P. Umari and A. Pasquarello, Phys. Rev. Lett. **89**, 157602 (2002).
[23] J. M. Ziman, *Principles of the Theory of Solids*, 2nd ed. (Cambridge University Press, Cambridge, 1972).
[24] B. Cichocki and B. U. Felderhof, Physica A **158**, 706 (1989).
[25] M. Holst and F. Saied, J. Comput. Chem. **14**, 105 (1993).
[26] M. J. Holst and F. Saied, J. Comput. Chem. **16**, 337 (1995).
[27] J.-L. Fattebert and F. Gygi, Int. J. Quantum Chem. **93**, 139 (2003).
[28] D. A. Scherlis, J.-L. Fattebert, F. Gygi, M. Cococcioni, and N. Marzari, J. Chem. Phys. **124**, 074103 (2006).
[29] W. L. Briggs, V. E. Henson, and S. F. McCormick, *A Multigrid Tutorial*, 2nd ed. (SIAM, Philadelphia, 2000).
[30] U. Trottenberg, C. W. Oosterlee, and A. Schüller, *Multigrid* (Academic, London, 2001).
[31] M. C. Payne, M. P. Teter, D. C. Allan, T. A. Arias, and J. D. Joannopoulos, Rev. Mod. Phys. **64**, 1045 (1992).
[32] Numerical Recipes (http://www.nrbook.com/).
[33] L. F. Greengard, *The Rapid Evaluation of Potential Fields in Particle Systems* (MIT, Cambridge, 1988).
[34] N. Marzari, Ph.D. thesis, University of Cambridge, 1996.
[35] N. E. Singh-Miller and N. Marzari (unpublished).
[36] B. Kozinsky and N. Marzari, Phys. Rev. Lett. **96**, 166801 (2006).
[37] M. Peressi, S. Baroni, A. Baldereschi, and R. Resta, Phys. Rev. B **41**, 12106 (1990).
[38] J. E. Jaffe and A. C. Hess, J. Chem. Phys. **105**, 10983 (1996).
[39] K. N. Kudin and G. E. Scuseria, Phys. Rev. B **61**, 16440 (2000).
[40] K. N. Kudin and G. E. Scuseria, J. Chem. Phys. **121**, 2886 (2004).
[41] N. D. Lang and W. Kohn, Phys. Rev. B **7**, 3541 (1973).
[42] M. Otani and O. Sugino, Phys. Rev. B **73**, 115407 (2006).
[43] D. Vanderbilt, Phys. Rev. B **41**, 7892 (1990).
[44] S. Baroni *et al.*, *Quantum-Espresso*, http://www.quantum-espresso.org/
[45] M. Holst *et al.*, *FETK*, http://www.fetk.org/